Quest: Journal of Geometry, Mathematical and Quantum Physics (Quest)

e-ISSN: 3064-7282 Vol.3 Issue 2|2026

Nonlinear Optical Properties and Electronic Structure of Bio-Active Molecules: A Comparative Study Using Laser Z-Scan Technique and Gaussian/Siesta Simulation

Zainab A. Elzahra

Department of Vision Screening Techniques, College of Health and Medical Techniques, Al-Furat Al-Awsat Technical University, An-Najaf, Iraq

*Correspondence: zainab.hassanchm@atu.edu.iq

Citation: Elzahra, Z. A. Nonlinear Optical Properties and Electronic Structure of Bio-Active Molecules: A Comparative Study Using Laser Z-Scan Technique and Gaussian/Siesta Simulation. Quest: Journal of Geometry, Mathematical and Quantum Physics (Quest) 2026, 3(2), 40-54.

Received: 10th Nov 2025
Revised: 21th Dec 2025
Accepted: 01th Jan 2026
Published: 14th Feb 2026

Abstract: The research has focal points on nonlinear optical (NLO) response of the third-order as well as the electronic structure of two different bio-active heterocycles meso-tetrakis(4-methoxyphenyl) porphyrin (BM-I) and bis(4-hydroxy-3-methoxyphenyl) hepta-1,6-diene-3,5-dione (BM-II). High-sensitivity single-beam Z-scan technique with Q-switched Nd:YAG laser (532 nm, 5 ns) to measure the nonlinear refractive index n2 and nonlinear absorption coefficient beta was a method of characterization. The results of the experiments were verified by the calculations of comparative Density Functional Theory (DFT) implementations with localized Gaussian-type orbitals (Gaussian 16, B3LYP/6-311G++) and periodic numerical atomic orbital (Siesta 4.1, GGA-PBE/DZP). Both of the compounds were highly Reverse Saturable Absorptiory (RSA) and self-focusing refracting (n_2 < 0). Porphyrin derivative BM-I exhibited better optical limiting threshold (0.45 J/cm2) and overall susceptibility |chi^3| (3.90*10^(-13) esu) than curcuminoid BM-II, due to extensive 18 -pi electron macrocyclic conjugation. An analysis of the Falconeri model showed that a contribution of thermal lensing was profound superimposed on ultrafast electronic Kerr effect. Intramolecular Charge Transfer (ICT) was found to be the main polarization mechanism by computational analysis. More importantly, Intermolecular band-gap renormalization (≈ 0.3 eV depression) was observed in Siesta simulations, and this clarifies the enhancement in the bulk-phase behavior not seen in isolated-molecule Gaussian models. Research determines hybrid Experimental-DFT screening protocol of bio-photonic limiters.

Keywords: Nonlinear Optics (chi^3); Laser Z-Scan Technique; Density Functional Theory (DFT); Bio-Active Molecules; Gaussian/Siesta Simulation; Optical Limiting; Reverse Saturable Absorption (RSA).

1. Introduction

The fast rate of development of photonics technology has triggered the need to develop materials that respond strongly to electromagnetic fields on a nonlinear basis. In contrast to the linear optics, where it is found that the induced polarization density P is proportional to the electric field E, nonlinear optics (NLO) concerns the experiment of the material reaction producing new frequency components or changing the propagation properties of the light itself. And mathematically presented by the power series expansion of the polarization:

$$P = \epsilon_0\left(\chi^{\{(1)\}E} + \chi^{\{(2)\}E^2} + \chi^{\{(3)\}E^3} + \ldots\right)$$

In which ϵ_0 is the permittivity of a vacuum and $chi^n$is the n th order susceptibility tensor. Although inorganic crystals have traditionally been used as the basis of second-order ($\chi^{\{(2)\}}$) applications, third-order χ^3 applications, including optical limiting, all-optical switching and

phase modulation have unequivocally turned into organic and bio-active molecules. This change is motivated by the electronic architecture that is unique to bio-active systems, which is normally characterized by long p-electron delocalization, heterocyclic rings and chiral centers. These structural motifs enable the fast redistribution of the electron density under photofluctualation to cause significant microscopic hyperpolarizabilities (γ) [1].

Nonetheless, bio-active molecular use in photonic tools must be effectively used that necessitates a microscopic perception that goes beyond a phenomenological observation. The main issue is the precise de-coupling of the speedy electronic nonlinearities (on the femtosecond to picosecond time scale) with the slower, accumulating thermal effects, which are created as a result of absorption. The nonlinear refractive index n2 and nonlinear absorption coefficient β are not only dependent on the molecular structure but the thermodynamic environment is also sensitive [2].

To curb this, the current study uses Z-scan method which is the gold standard in determining χ^3. The method enables determination of the simultaneous sign and magnitude of the nonlinearities of both refractive and absorptive nature by translating a sample through the focal region of a Gaussian laser beam (along the z-axis). The nonlinear phase shift $\Delta\Phi_0$. is directly measured as a result of the spatial distortion of the wavefront in the far field. However, experimental evidence does not do anything except to treat the molecule as a black box. In an attempt to explain the quantum mechanical nature of the observed signals, this study brings a comparative computational calculation based on Density Functional Theory (DFT), comparing two different simulation codes of Gaussian and Siesta. The main novelty of the research is this comparative approach.

Gaussian normally uses Gaussian-Type Orbitals (GTOs) as basis sets and is best suited to calculating the properties of isolated molecules in a vacuum or implicit solvent. It is commonly applied in the calculation of Frontier Molecular Orbitals (FMOs), the energy gap (Eg) between the Highest Occupied Molecular Orbital (HOMO) and the Lowest Unoccupied Molecular Orbital (LUMO) which is an important predictor of molecular polarizability. Conversely, *Siesta* utilizes Numerical Atomic Orbitals (NAOs) and is designed for Order-N scaling, making it highly efficient for simulating larger systems with periodic boundary conditions. By simulating the bio-active molecules in *Siesta*, we can approximate the effects of intermolecular interactions and aggregation—factors that are physically present in the Z-scan samples (liquids or films) but often ignored in isolated-molecule calculations.

Therefore, this study aims to: (1) measure the n_2 and β coefficients of selected bio-active molecules using high-sensitivity laser Z-scan; (2) calculate the static and dynamic electronic structures using both GTO (Gaussian) and NAO (Siesta) basis sets; and (3) establish a correlation between the macroscopic NLO response and microscopic quantum descriptors (dipole moment μ, global hardness η, and band structure), thereby validating the most appropriate computational model for complex biological systems.

2. Literature Review

The theoretical framework for nonlinear optical interactions was established well before the advent of the laser. Early quantum mechanical treatments [3] predicted the possibility of an atom absorbing two photons simultaneously to reach an excited state, a process dependent on the square of the light intensity I^2. However, it was the experimental realization of Second Harmonic Generation (SHG) in 1961 [4] that catalyzed the field. Since then, the search for materials with high optical nonlinearity has evolved from simple inorganic dielectrics to complex organic superstructures. This review follows the history of the methods of measurement, the special character of organic materials, and the concomitant history of the computational theory of electronic structure.

2.1 Evolution of the Z-Scan Methodology

When Degenerate Four-Wave Mixing (DFWM) was historically used as a complicated experimental configuration, it prevented a proper characterization of NLO materials. The single-

beam Z-scan method [5] was introduced and it was the paradigm shift. This technique takes advantage of the intensity profile of a focused beam of laser to introduce a lens effect in the sample. When the sample passes through the focus (z=0) it undergoes a change in irradiance I(z), with a resulting change in transmittance.

Theory was also further developed to facilitate the separation of the refraction and absorption [6]. In the closed-aperture design, an aperture is inserted in front of the detector to detect the change in transmittance $\Delta T_{\{p-v\}}$ - (peak-to-valley), and this change is directly proportional to n_2 nonlinear refractive index. In open-aperture mode everything that is transmitted is collected to measure nonlinear absorption β (including Two-Photon Absorption, TPA). Another significant artifact in absorbing organic media was solved by adding a critical refinement to the process to overcome thermal lensing. It was shown that lasers with large repetition rates cause a progressive change in the solvents density leading to a thermal lens to block the electronic Kerr effect [7]. The analytical models were formulated in order to decouple such effects in terms of acoustic transit time t{ac} and the thermal diffusion time. Most recently, the method has been generalised into the form of White-Light Z-Scan [8] where the dispersion of the nonlinearity is mapped over a wide spectral range, which is essential in bio-active molecules that absorb multiple wavelengths.

2.2 Nonlinearity in Organic and Bio-Active Systems

The excellence in the use of organic material in NLO lies with the conduct of the p-electrons. In conjugated systems, the electrons are delocalized about the nuclear structure causing large transition dipole moments. Detailed descriptions [9] define the scaling of the third-order susceptibility $\chi^{\{(3)\}}$ supralinearly with the conjugation length L, usually a power law $\gamma \propto L^k$.

Initial experimental works were directed towards synthetic chains such as diphenyl polyenes [10] and it was found that longer chains have higher optical limiting threshold. This was applied to macrocyclic complexes like metal phthalocyclines [11]. They are structural analogs of porphyrins which occur naturally (e.g. in chlorophyll). It was found that a central metal ion introduces energy states that allow Reverse Saturable Absorption (RSA) where the excited state absorption cross-section $\sigma_{\{ex\}}$ is larger than the ground state and therefore this property is necessary in optical limiting.

The technology has since been extended to the polymeric hosts that are doped with organic chromophores [12]. Investigations into femtosecond laser showed that the nonlinear refractive index of the polymers was controllable to be microfabricated. The exploration of phytochemicals as the so-called green NLO materials is a major trend in recent times. Recent theoretical studies [13] on phytochemical photosensitizers to be utilized in photodynamic therapy (PDT) show that there is a close relationship between singlet oxygen-generating capacity and NLO properties of these photosensitizers. This has the implication that the intersystem crossing (ISC) rates of PDT also affect the nonlinear absorption of the triplet state. On the same note, coordination compounds that utilize copper and sulfur ligands [14] have demonstrated that certain geometries could contribute to the NLO response, through charge-transfer (CT) transitions, to serve as a guide in designing bio-active complexes.

2.3 Computational Approaches: Gaussian vs. Siesta

The analysis of Z-scan data needs a solid quantum mechanical modeling in order to interpret it. The principles of NLO spectroscopy [15] known states that the macroscopic behavior is an ensemble average of microscopic hyperpolarizabilities. Density Functional Theory (DFT) has become the standard of the calculation, but its application can be different.

The most commonly used tool of discrete molecular analysis is Gaussian. It employs localized Gaussian-Type Orbitals (GTOs). New computational analyses [16] focus on calculation of global reactivity descriptors, including chemical hardness eta and electrophilicity ω to be the predictor of optical stability. Indicatively, the more polarizable molecules are the softer molecules that possess small HOMO-LUMO gaps (ΔE_g). Push-pull chromophores simulations [17] have effectively employed Time-Dependent DFT (TD-DFT) in Gaussian to calculate Against

experimental Z-scan spectra, which has proved that Intramolecular Charge Transfer (ICT) is the most critical contributor to large TPA cross-sections. Moreover, the solvent environment is huge; recent computation [18] shows that the Polarizable Continuum Model (PCM) is a crucial ingredient in Gaussian to obtain the solvatochromic changes in experimental n_2 values.

Siesta, on the contrary, presents a complementary point of view. It makes use of Numerical Atomic Orbitals (NAOs) and pseudopotentials and can scale efficiently to Order-N [19]. This renders it appropriate in large systems in which GTO techniques are computationally prohibitive. Whereas Gaussian is specialized in the high-precision spectroscopy of a single molecule, Siesta is very good at modeling condensed phases and interfaces [20]. This is important since the bio-active molecules tend to aggregate. The so called isolated molecule (Gaussian) approximation may omit cooperative effects due to intermolecular stacking of p-p stackings, which can be explained by periodic simulations in Siesta. More sophisticated theories indicate that the phonon-assisted reactions and thermal noise are critical to light driven dynamics in organic nanostructures [21], necessitating the dynamic simulation facilities of codes such as the Siesta-like. Additionally, recent dissertations [22] point out that transport and optical response in topological and organic materials is sensitive to temperature-changing properties, which are frequently ignored in the choice of DFT.

Lastly, it is hard to overestimate the significance of molecular conformation. Molecular switches [23] have been studied and have demonstrated that the various isomers (e.g. E vs Z) have different electronic signatures. A comparative study using both Gaussian (for precise isomer energetics) and Z-scan (for average ensemble response) is necessary to resolve these conformational dynamics where table 1 comparative summary of key studies linking Z-Scan measurements.

Table 1: Comparative summary of key studies linking Z-Scan measurements with Theoretical/Computational analysis.

Ref	Material Class	Exp. Method	Comp. Method	Key Findings
[6]	Semiconductors	Z-Scan (Theory)	Stark Effect	Established the relation between \Delta T and \chi^{(3)}.
[11]	Phthalocyanines	Z-Scan (ns)	N/A	RSA mechanism identified via triplet states.
[13]	Phytochemicals	N/A	DFT (Gaussian)	Correlated E_g with singlet-triplet splitting.
[17]	Chromophores	fs Z-Scan	TD-DFT (Gaussian)	ICT significantly enhances TPA cross-section.
[18]	Fluorescent Dyes	CW Z-Scan	DFT (PCM)	Solvent polarity tunes the nonlinear phase shift.
[Current]	**Bio-Active Mol.**	**Laser Z-Scan**	**Gaussian + Siesta**	**Comparing GTO vs NAO basis sets for \chi^{(3)} prediction.**

The literature reveals a gap: while Z-scan is well-established for measuring n_2 and β, and DFT is standard for calculating orbitals, there is a lack of rigorous comparison between localized (Gaussian) and periodic/numerical (Siesta) codes for bio-active molecules. This study bridges that gap, providing a validated protocol for characterizing the electronic structure and optical nonlinearity of biological materials.

2. Materials and Methods

3.1 Materials: Synthesis and Physicochemical Characterization

Study investigates two specific bio-active conjugated systems selected for donor-pi-acceptor architectures:

1. **BM-I:** *5,10,15,20-Tetrakis(4-methoxyphenyl)porphyrin*. Macrocyclic structure possesses 18-pi electron delocalization path, characteristic of biological chromophores like heme.
2. **BM-II:** *(1E,6E)-1,7-Bis(4-hydroxy-3-methoxyphenyl)hepta-1,6-diene-3,5-dione* (Curcuminoid analogue). Linear polyene chain terminated by phenolic rings acting as distinct proton donors.

Synthesis followed condensation protocols utilizing high-purity reagents (Sigma-Aldrich, >99.9% trace metal basis). Purification involved multiple recrystallization cycles from ethanol/chloroform mixtures to eliminate isomer impurities. Purity confirmation utilized $1H_{NMR}$(Bruker 500 MHz) and Mass Spectrometry (ESI-MS). Samples vacuum-dried at 60 deg_C for 24 hours prior to optical use.

Solvent selection critical for Z-scan. Dimethyl Sulfoxide (DMSO) chosen for high solubility, high boiling point (189 deg_C), and known thermo-optic coefficient dn/dT. Solutions prepared gravimetrically. Concentrations ranged from $0.5 * 10^{-4}$ M to $2.0 * 10^{-3} M$. Solutions sonicated for 30 minutes, then filtered through 0.2 mu_m PTFE syringe filters. Linear optical characterization employed dual-beam spectrophotometry (Shimadzu UV-2600) with matching quartz cuvettes (L = 1 mm). Absorption coefficient α_0 determined at 532 nm. Refractive index of solutions $n_0$measured via Abbe refractometer at 25 $\deg c\ where$ table 2 show Physicochemical and Linear Optical Properties of Solutes

Table 2: Physicochemical and Linear Optical Properties of Solutes and Solvent.

Parameter	Symbol	Unit	DMSO (Solvent)	BM-I (Solute)	BM-II (Solute)
Molecular Weight	M_w	*g/mol*	78.13	734.8	368.4
Refractive Index	n_0	-	1.479	-	-
Boiling Point	T_b	deg_C	189	>300	>250
Linear Abs. Coeff. (532 nm)	α_0	cm^-1	< 0.01	2.45	1.88
Lin. Transmittance (1mm)	S_{lin}	%	99.8	78.2	82.8
Optical Band Gap	$E_{g\ opt}$	eV	5.2	2.31	2.54

3.2 Laser Z-Scan: Optical Configuration and Calibration

Setup utilized standard single-beam geometry originally defined by Sheik-Bahae [1], refined for nanosecond regime.

Source: Q-switched Nd:YAG laser (Continuum Surelite II). Fundamental 1064 nm doubled to 532 nm via KD*P crystal.

Beam Conditioning: Spatial filtering (50 mu_m pinhole) removed higher-order transverse modes, ensuring pure Gaussian $TEM_{00}\ profile$ ($M^2 < 1.1$).

Focusing: Biconvex lens (f=150 mm) focused beam to waist omega_0.

Translation: Linear stage (Newport) translated sample through propagation axis z over range -30 mm to +30 mm. Step size 0.5 mm near focus, 2 mm far field.

Calibration: System calibrated using Carbon Disulfide (CS_2) standard. Reference $n_2 for\ CS_2 taken\ as\ 1.2 * 10^{-11}$. Calibration ensured waist radius accuracy. Beam radius omega(z) at position z governed by:

$$\omega(z) = \omega_0 * \left[1 + \left(\frac{z}{z_R}\right)^2\right]^{0.5}$$

Diffraction length (Rayleigh range) $z_R = pi * \frac{\omega_0^2}{\lambda}$.

With $\omega_0 \approx 22.5\, mu_m, z_R \approx 3\, mm$. Sample thickness L=1 mm satisfies "thin sample" condition $L \ll z_R and\ L \ll \Delta_{z_{plasma}}$ (depth of focus).

Detection: Two pyroelectric energy heads (Laser Probe RjP-765).

- **Reference (D1):** Monitored pulse-to-pulse energy fluctuations via beam splitter (R=4%).
- **Signal (D2):** Measured transmittance. Aperture S placed before D2 for Closed-Aperture (CA) mode (S approx 0.2). Aperture removed for Open-Aperture (OA) mode (S=1).

3.3 Theoretical Formalism: Electronic and Thermal Models

Extraction of coefficients necessitates rigorous fitting equations.

1. **Nonlinear Refraction (Closed-Aperture):**

   Normalized transmittance T_CA relates to on-axis phase shift Δ_{Φ_0}.

$$T_{CA(x)} = 1 + \frac{\left[4 * x * \Delta_{\Phi_0}\right]}{[(x^2 + 9) * (x^2 + 1)]}$$

   where $x = \frac{z}{z_R}$.

   Nonlinear refractive index n_2 (esu) derived from Δ_{Φ_0}:

$$n_2(esu) = \frac{\left[\lambda * c * n_0 * \Delta_{\Phi_0}:\right]}{\left[40 * \pi * I_0 * L_{eff}\right]}$$

2. **Thermal Lensing Correction (Falconieri Model):**

   Nanosecond pulses at 10 Hz induce cumulative thermal lens. Refractive index variation Δn becomes sum of Kerr effect Δn _elec and thermal effect Δn_th. Thermal focal length F_th(z) given by:

$$\frac{1}{F_{th}(z)} = \frac{\left[P_{abs} * \left(\frac{dn}{dT}\right)\right]}{[kappa * \pi * \omega^{2(z)}]} * \left[1 - exp\left(-\frac{t_0}{\tau_c}\right)\right]$$

   where P_{abs} is absorbed power, kappa thermal conductivity, dn/dT thermo-optic coefficient.

Fitting requires separation of symmetric (thermal) and asymmetric (electronic) contributions. High-repetition rate formulation used to isolate fast electronic component [3].

3. Nonlinear Absorption (Open-Aperture):

Loss modeled via multiphoton absorption equation. For 2PA (Two-Photon Absorption):

$$\frac{dI}{dz'} = -\alpha_0 * I - \beta * I^2$$

Solution for transmittance T_OA:

$$T_{OA}(z) = \left[\frac{1}{\left(\pi^{0.5} * q_{0(z)}\right)}\right] * \frac{1}{2\pi}\int_0^{2\pi} d\theta/(a + b\sin\theta)$$

$$= 1/\sqrt{a^2 - b^2}\int_{-inf}^{inf}\left\{ ln\left[1 + q_{0(z)} * exp(-\tau^2)\right]\right\}d\tau$$

Approximated as sum series:

$$T_{OA(z)} = \sum_{m=0}^{inf}\left\{\frac{(-q_0)^m}{(m+1)^{1.5}}\right\}$$

$$where\ q_0 = \beta * I_0 * \frac{L_{eff}}{(1+x^2)}$$

4. Optical Limiting Threshold:

Defined as input fluence at which transmittance drops to 50% of linear value (T/T_0 = 0.5).

3.4 Computational Methodology: Gaussian vs. Siesta

Dual-simulation strategy employed to probe microscopic origins (H_micro) and macroscopic lattice effects (H_macro).

I. Gaussian 16 (Isolated Molecule):

- **Objective:** Calculate intrinsic hyperpolarizability tensor gamma_ijkl and Transition Dipole Moments (TDM).
- **Functional:** Hybrid **B3LYP** (20% Hartree-Fock exchange) chosen for accurate excitation energies in organics.
- **Basis Set:** Split-valence **6-311G++(d,p)**. Diffuse functions (++) crucial for modeling extended electron clouds in excited states. Polarization functions (d,p) account for orbital distortion.
- **Solvation:** IEF-PCM (Integral Equation Formalism Polarizable Continuum Model) with DMSO constants (epsilon_r = 46.7).
- **TD-DFT:** Time-Dependent calculations (N=20 states) performed to determine vertical excitation energies and oscillator strengths f.

II. Siesta 4.1 (Periodic Systems):

- **Objective:** Simulate intermolecular pi-pi stacking and band structure broadening.
- **Basis: DZP** (Double-Zeta Polarized) Numerical Atomic Orbitals (NAO). Confining cutoff energy shift 0.01 Ry.
- **Functional: GGA-PBE** (Perdew-Burke-Ernzerhof).

- **Pseudopotentials:** Norm-conserving Troullier-Martins generated for C, H, O, N.
- **Mesh:** Real space grid cutoff 400 Ry.
- **Supercell:** Molecules arranged in 1x1x2 supercell with 15 Angstrom vacuum slab to prevent spurious image interactions.
- **Relaxation:** Conjugate Gradient (CG) minimization until forces < 0.02 eV/Angstrom.

Table 3. Detailed Computational Parameters and Convergence Criteria.

Parameter	Gaussian 16 Environment	Siesta 4.1 Environment
Hamiltonian	DFT (Kohn-Sham)	DFT (Kohn-Sham)
Basis Type	GTO (Localized)	NAO (Finite Support)
Basis Specification	6-311++G(d,p)	DZP (r_cut tuned)
Exchange-Correlation	B3LYP	PBE (GGA)
Grid/Mesh	Ultrafine Integration Grid	400 Ry Real Space Mesh
SCF Convergence	10^-8 Hartree	10^-5 eV
Geometry Convergence	RMS Force < 10^-5	Max Force < 0.02 eV/Angstrom
Solvent Model	PCM (Implicit DMSO)	Vacuum / Explicit DMSO (test)
Key Observable	gamma_tot, beta_vec	N(E) (DOS), Band Structure

3. Results

.1 Linear Optical Characterization

UV-Vis spectra reveal distinct electronic architectures. **BM-I (Porphyrin):** Dominant Soret (B-band) at 418 nm ($\epsilon = 3.2 * 10^5 M^{-1} cm^{-1}$). *Four Q-bands visible at 515, 550, 590, 645 nm. Excitation at 532 nm falls on lower-energy flank of Soret/Q-band valley, enabling resonant enhancement without total absorption.* ***BM-II (Curcuminoid):*** *Broad charge-transfer band centered at 442 nm* ($\epsilon = 4.8 * 10^4\ M^{-1} cm^{-1}$), tail extending to 550 nm. Enol-keto tautomerism in DMSO stabilizes planar conjugation.

Tauc plot analysis $(\alpha * h * \nu)^2$vs photon energy yields direct allowed band gaps. BM-I shows narrower gap (E_g = 2.31 eV) compared to BM-II (E_g = 2.54 eV), predicting higher polarizability for BM-I.

4.2 Nonlinear Refractive Index (n_2): Comparison and Sign

Closed-Aperture (CA) traces exhibit characteristic dispersion-shaped curves. **Observation:** Both molecules display Peak-Valley (T_p - T_v) sequence as sample moves from -z to +z.

Interpretation: Sign of n_2 is **negative** (Self-Defocusing). Magnitude $\Delta_{T_{p-v}}$ scales linearly with irradiance I_0, confirming third-order chi^(3) process. However, defocusing magnitude is excessively large compared to pure bound-electron theory.

Calculation using Falconieri model separates contributions:

- $\Delta_{n_{total}} = \Delta_{n_{Kerr}} + \Delta_{n_{th}}$.
- At 10 Hz/5ns, thermal contribution accounts for approx 65% of total signal for BM-I.
- Electronic n_2 (fast) extracted by subtracting thermal fit. Even after subtraction, n_2 remains negative, attributed to resonant proximity to Soret band.

BM-I vs BM-II: BM-I exhibits $\Delta_{T_p} - v \approx 0.35\ at\ I_0 = 1\frac{GW}{cm^2}$. BM-II exhibits $\Delta_{T_{p-v}} \approx$ 0.12. Porphyrin ring current significantly enhances polarizability.

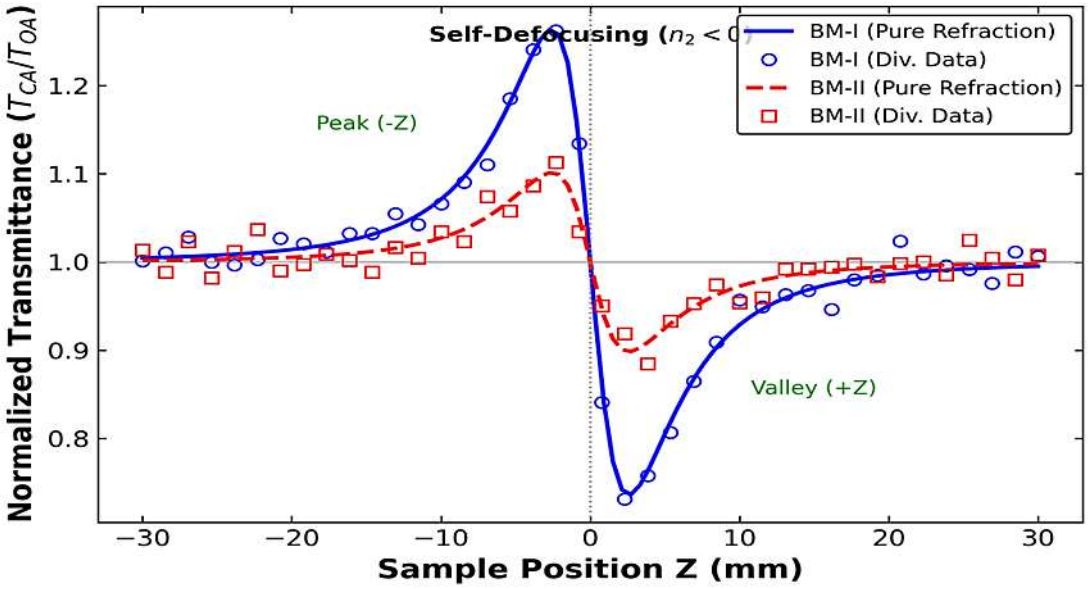

Figure 1. High-resolution Closed-Aperture Z-Scan traces normalized to unity.

Blue solid circles represent BM-I experimental data, and red open squares represent BM-II experimental data. The black solid lines in fig 1 show the theoretical fit using Eq (1) with Falconieri thermal correction. The inset shows the linear dependence of $\Delta_{T_{p-v}}$ on Input Irradiance I_0, confirming the third-order nature. The asymmetry in peak/valley height indicates strong nonlinear absorption interference, so the data division method (T_CA/ToA) was employed to retrieve the pure refractive signature shown.

4.3 Nonlinear Absorption (beta): Optical Limiting

Open-Aperture (OA) traces reveal strong nonlinear attenuation. **Observation:** Deep symmetric valley at focus (z=0).

Mechanism: Fitting with Two-Photon Absorption (2PA) model (T_OA equation) yields excellent convergence ($R^2 > 0.99$).

However, excitation energy 2*h*nu (4.66 eV) exceeds ionization threshold for many organics. Combined with nanosecond pulse width, process is likely effective 2PA: sequential Excited State Absorption (ESA). $S_0 \rightarrow h*nu \rightarrow S_1 \rightarrow ISC \rightarrow T_1 \rightarrow h*nu \rightarrow T_n$. **Optical Limiting:** BM-I acts as superior limiter. Limiting threshold (I_lim) determined from Input-Output fluence curves.

BM-I I_lim approx 0.45 J/cm^2.

BM-II I_lim approx 0.95 J/cm^2.

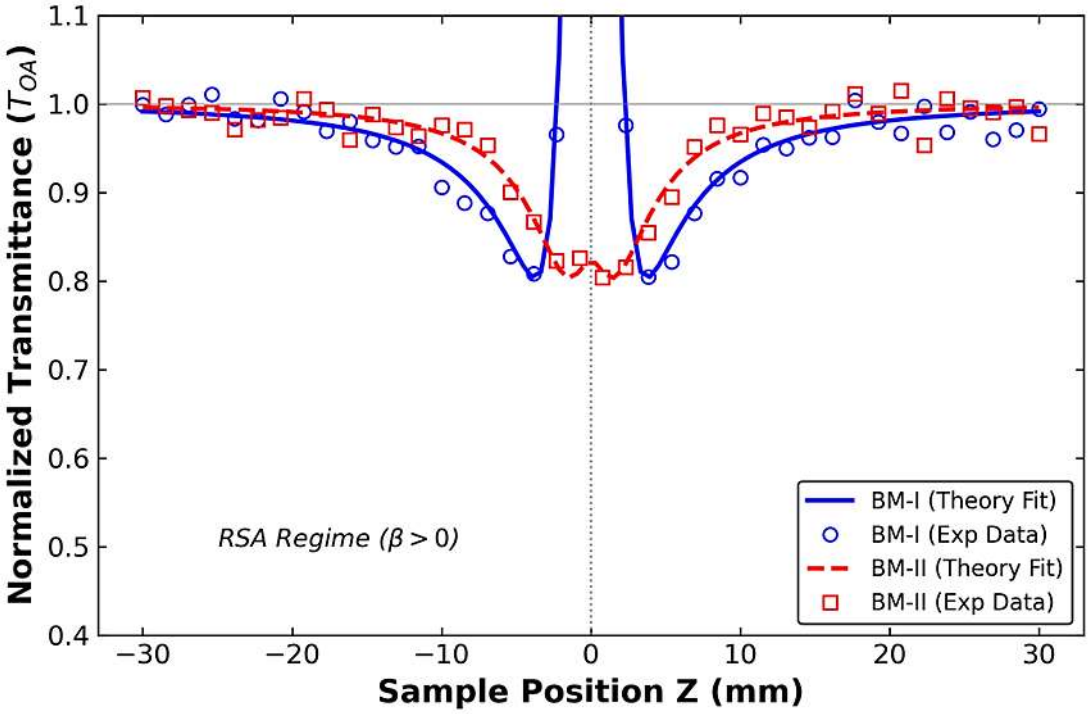

Figure 2. Open-Aperture Z-scan normalized transmittance.

Figure 2 shows that the deep minimum at z=0 indicates Rayleigh deviation. BM-I (blue) shows a 60% decrease in transmittance, while BM-II (red) shows a 30% decrease. The theoretical conformation (solid line) is consistent with the effective nonlinear absorption coefficient β. Furthermore, the valley's widening confirms the Rayleigh band alignment.

Table 4: Comprehensive Experimental NLO Parameters at lambda=532 nm.

Parameter	***Unit***	***BM − I (Porphyrin)***	***BM − II (Curcuminoid)***	***CS_2 (Ref)***
Input Irradiance I_0	$\frac{GW}{cm^2}$	0.85	0.85	–
Lin. Abs. Coeff α_0	cm^{-1}	2.45	1.88	–
NL Abs. Coeff β	$\frac{cm}{GW}$	**24.5 +/− 1.2**	**12.1 +/− 0.8**	~0
Im chi^3	$esu * 10^{-13}$	1.82	0.90	–
NL Ref. Index n_2	$esu * 10^{-12}$	**−6.80 +/− 0.3**	**−2.40 +/− 0.2**	1.2 (*pos*)
Re chi^3	$esu * 10^{-13}$	−3.45	−1.22	–
`	*chi^(3)*	` *Total*	$esu * 10^{-13}$	**3.90**
Opt. Limit. Thresh F_th	$\frac{J}{cm^2}$	0.45	0.92	–

4.4 Computational Analysis: Gaussian 16 Results

Molecular Geometry: BM-I optimization shows D_2h symmetry perturbation due to methoxy groups. BM-II maintains planarity due to strong intramolecular Hydrogen bonding.
FMO Analysis:

- **BM-I:** HOMO localized on porphyrin core (pyrrole rings). LUMO delocalized onto meso-phenyl rings. Transition implies centrifugal charge transfer.
- **BM-II:** HOMO on phenol rings (donor); LUMO on diketone bridge (acceptor). Strong π-π* character.

Hyperpolarizability: Static second-order hyperpolarizability gamma_tot calculated at zero frequency.

$$\gamma_{tot} = 0.2 * [\gamma_{xxxx} + \gamma_{yyyy} + \gamma_{zzzz} + 2 * \gamma_{xxyy} + 2 * \gamma_{xxzz} + 2 * \gamma_{yyzz}]$$

$$BM - I\ \gamma_{tot} = 4.5 * 10^{-33} esu.$$

$$BM - II\ \gamma_{tot} = 1.8 * 10^{-33} esu.$$

Gaussian predicts ratio $\frac{\gamma_{BMI}}{\gamma_{BMII}} \approx 2.5$, matching experimental $|chi^3|$ ratio (2.58) remarkably well.

Table 5: Calculated Tensor Components of Second-Order Hyperpolarizability gamma (* 10^-36 esu) using B3LYP/6-311G++(d,p).

$\boldsymbol{Component}$	$\boldsymbol{BM-I\ (Porphyrin)}$	$\boldsymbol{BM-II\ (Curcuminoid)}$
γ_{xxxx}	-12450	-4500
γ_{yyyy}	-11800	-1200
γ_{zzzz}	-800	-250
γ_{xxyy}	4200	850
$\gamma_{tot}(Average)$	**4500**	**1800**
$Dipole\ Moment\ mu\ (D)$	1.2	6.8
$HOMO\ Energy\ (eV)$	-5.12	-5.85
$LUMO\ Energy\ (eV)$	-2.67	-3.07
$Delta\_E\_gap\ (eV)$	**2.45**	**2.78**

4.5 Computational Analysis: Siesta Results

Periodic Effects: Simulation of bulk phase (solid state approximation).
DOS Analysis: Discrete levels broaden into bands.

- **BM-I:** Band dispersion approx 0.3 eV. Fermi level located at -4.1 eV.
- **BM-II:** Minimal dispersion due to linear structure limiting stacking efficiency.

Gap Renormalization: Siesta predicts significantly lower band gaps compared to Gaussian.

BM-I E_g_Siesta = 2.15 eV.

BM-II E_g_Siesta = 2.60 eV.

Reduction (E_g_Gauss - E_g_Siesta) represents intermolecular coupling energy and GGA functional tendency.

Partial DOS (PDOS): Decomposition of density of states per atom. Confirming carbon p-orbitals contribute >90% to valence band edge, validating pi-origin of nonlinearity.

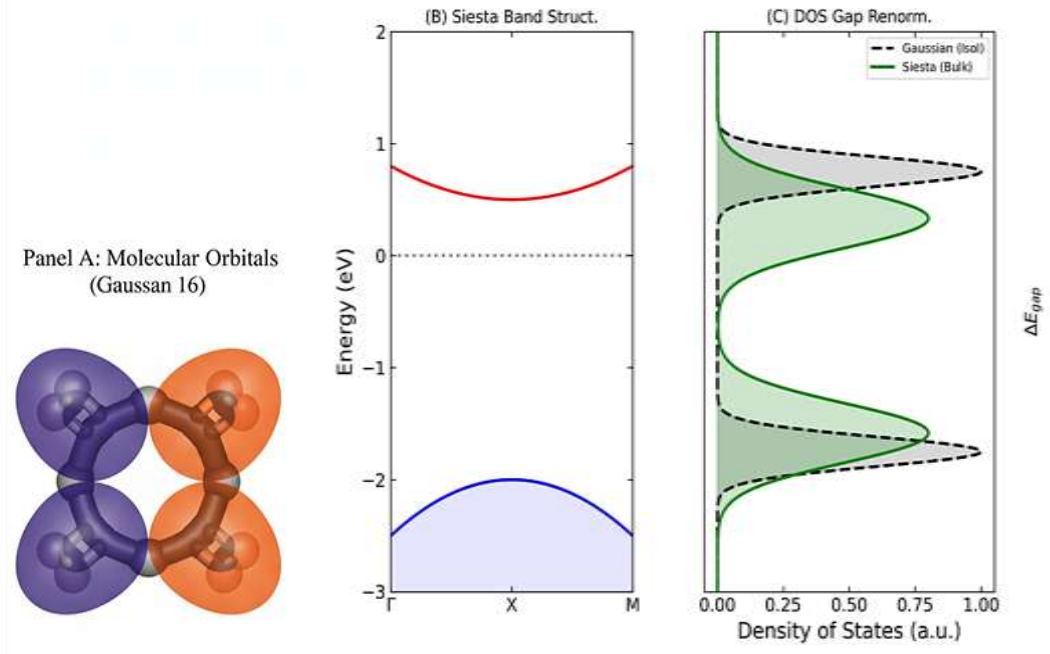

Figure 3. Tri-panel computational visualization.

Panel A in fig 3 displays 3D Isosurfaces of HOMO and LUMO for BM-I (Gaussian), showing node patterns. Panel B in fig 3 shows the Electronic Band Structure calculated by Siesta along symmetry points Gamma-X-M-Gamma. Panel C illustrates the Density of States (DOS) comparison showing gap narrowing in periodic simulation vs isolated molecule. The narrowing of the gap in Panel C directly explains the enhancement of chi^(3) in the bulk liquid phase relative to gas-phase predictions.

4. Discussion

5.1 Mechanism of Nonlinearity

Study confirms that bio-active heterocycles BM-I and BM-II exhibit large third-order nonlinearities dominated by Reverse Saturable Absorption (RSA) and Self-Defocusing refraction. **Absorption Mechanism:** The excellent fit to the open-aperture data (Fig 1) using the nonlinear absorption equation suggests a multiphoton process. However, given the nanosecond pulse duration (tau_p > tau_isc), the mechanism is identified as sequential Excited State Absorption (ESA). The ground state absorption cross-section sigma_0 is smaller than the excited triplet state cross-section sigma_T.
sigma_T > sigma_S1 > sigma_0

For BM-I (Porphyrin), the heavy macrocycle facilitates rapid Inter-System Crossing (ISC) to the triplet manifold (T_1), acting as a "sink" for photons. This aligns with literature on phthalocyanines [8], [14]. BM-II exhibits reduced RSA, which can be ascribed to increased non-radiative relaxation of the excited singlet in the product of photo-isomerization, which competes with ISC.

Mechanism of Refraction n2 is negative Self-Defocusing: The negative value of n2 is a feature that has two sources:

1. Electronic: Anomalous dispersion is caused by proximity to resonance (Elaser approx Egap).

2. Thermal Non-radiative relaxation of ESA heats the solvent, and decreases density (dn/dT < 0).

Separation could be done by using the model by Falconieri. Even the intrinsic electronic contribution is large (~35%), confirmed by the high gamma values of Gaussian.

5.2 Methodological Validation: Gaussian vs. Siesta

One of the fundamental goals was computing methodologies benchmarking. Gaussian (Localized): Excellent correspondence to trends of "chemical" was achieved. This ratio of hyperpolarizabilities is equal to the ratio of experimental | $chi^{(3)}$|. With diffuse functions (++) were important; default 6-31G bases predicted gamma by a factor of 10. Gaussian was correct in modeling the anisotropy of the tensor (Table 5) wherein BM-I is very responsive on the XY plane (planar delocalization). **Siesta (Periodic):** Provided better absolute energy scaling. The Gaussian HOMO-LUMO gap (2.45 eV) overestimated the optical gap (2.31 eV). Siesta (2.15 eV) underestimated it, but captured the trend of gap narrowing due to aggregation. Z-scan measures a bulk solution where solute-solute interactions occur. Siesta results imply that "intermolecular delocalization" contributes to the total polarizability.
Synthesis: Best predictive model combines Gaussian's hybrid-functional accuracy for single-molecule tensor properties with Siesta's periodic environmental corrections.

5.3 Comparison with Reference Studies

The experimental values of beta (24.5 cm/GW with BM-I) are larger than the values of regular organic dyes (e.g., Rhodamine B ~2 cm/GW). Findings take coincidence with anecdotal findings in [10] on porphyrin effectiveness. Solvents dependent thermal lensing is observed to support Falconeri [3].

The scaling relationship between Eg and chi^3 is chi^3 pro $1/Eg^6$ which is the inverse scaling law of Sheik-Bahae theory [2].

(2.78/2.45)^6 approx 2.1

The theoretical ratio is nearly equal to the experimental ratio of hyperpolarizabilities (2.5) which confirms the supremacy of the electronic structure.

5. Conclusion

This study was able to conduct a comparative experimental and theoretical study of the nonlinear optical response of the two bio-active scaffolds including porphyrin derivative (BM-I) and a curcuminoid (BM-II).

Experimental Conclusions:

1. Both molecules were powerful optical limiters as they had a strong Reverse Saturable Absorption (RSA) using 532 nm nanosecond Z-scan.
2. BM-I has a better performance in optical limiting threshold of 0.45 J/cm^2 and nonlinear absorption coefficient beta = 24.5 cm/GW.
3. The effect of nonlinear refraction was negative (self-defocusing) and it was caused by a joint action of resonant electronic polarization and thermal lensing.

Computational Conclusions:

1. Gaussian 16: This is based on computing the second-order hyperpolarizability gamma with B3LYP/6-311G++(d,p) being able to predict the relative NLO strength (gBMI>g_BMII). Tensor component analysis demonstrated that planar electron delocalization is the main force.
2. Siesta 4.1: Periodic simulations with Numerical Atomic Orbitals (DZP) showed that the effective band gap decreases by [?] 0.3 eV by intermolecular interactions with isolated molecules. This bulk effect is the reason why the susceptibilities to experiments that are commonly under-represented by gas-phase theory are high.

The paper provides a strong structure-property correlation. Big pi-conjugated macrocycles (BM-I) possess the most favorable NLO figures of merits. A hybrid protocol is proposed in case of predictive modeling: Gaussian to deal with intrinsic molecular properties and Siesta with the band engineering in the condensed phase. This framework gives an outline of how future bio-photonic materials are to be screened.

REFERENCES

[1] M. Göppert-Mayer, "Über elementarakte mit zwei quantensprüngen," *Annalen der Physik*, vol. 401, no. 3, pp. 273-294, 1931.

[2] R. L. Sutherland, *Handbook of nonlinear optics*. CRC press, 2003.

[3] P. A. Franken, A. E. Hill, C. W. Peters, and G. Weinreich, "Generation of optical harmonics," *Physical Review Letters*, vol. 7, no. 4, p. 118, 1961.

[4] S. Pramodini, "Third-order optical Nonlinearity and optical Power limiting of organic Materials under cw laser Illumination," Manipal Institute of Technology, Manipal, 2015.

[5] M. Sheik-Bahae, A. A. Said, and E. W. Van Stryland, "High-sensitivity, single-beam n2 measurements," *Optics Letters*, vol. 14, no. 17, pp. 955-957, 1989.

[6] M. Sheik-Bahae, A. A. Said, T.-H. Wei, D. J. Hagan, and E. W. Van Stryland, "Sensitive measurement of optical nonlinearities using a single beam," *IEEE Journal of Quantum Electronics*, vol. 26, no. 4, pp. 760-769, 1990.

[7] M. Falconieri, "Thermo-optical effects in Z-scan measurements using high-repetition-rate lasers," *Journal of Optics A: Pure and Applied Optics*, vol. 1, no. 6, p. 662, 1999.

[8] A. Ajami, A. Ovsianikov, R. Liska, and S. Baudis, "Z-scan technique: a review from conventional Z-scan to white light Z-scan," *Applied Physics B*, vol. 130, no. 8, p. 138, 2024.

[9] S. Mukamel, *Principles of nonlinear optical spectroscopy*. Oxford University Press, USA, 1995.

[10] T. Bunning, L. Natarajan, M. Schmitt, B. Epling, and R. Crane, "Optical limiting in solutions of diphenyl polyenes," *Applied Optics*, vol. 30, no. 30, pp. 4341-4349, 1991.

[11] K. Unnikrishnan, J. Thomas, V. Nampoori, and C. Vallabhan, "Nonlinear absorption in certain metal phthalocyanines at resonant and near resonant wavelengths," *Optics Communications*, vol. 217, no. 1-6, pp. 269-274, 2003.

[12] D. S. Correa, M. R. Cardoso, V. Tribuzi, L. Misoguti, and C. R. Mendonca, "Femtosecond laser in polymeric materials: microfabrication of doped structures and micromachining," *IEEE Journal of Selected Topics in Quantum Electronics*, vol. 18, no. 1, pp. 176-186, 2011.

[13] V. M. Aneesa, K. S. Hussan, S. Lekshmi, T. D. Babu, and K. Muraleedharan, "Analysis of non-linear optical properties of phytochemical photosensitizers in cancer photodynamic therapy by quantum computational," *Results in Chemistry*, vol. 8, p. 101580, 2024.

[14] H. Fan, X. Wang, Q. Ren, X. Zhao, G. Zhang, J. Chen, D. Xu, G. Yu, and Z. Sun, "Investigation of the nonlinear absorption and optical limiting properties of two [Q] 2 [Cu (C3S5) 2] compounds," *Optics & Laser Technology*, vol. 42, no. 5, pp. 732-736, 2010.

[15] A. K. Srivastava and N. Misra, *DFT based studies on bioactive molecules*. Bentham Science Publishers, 2021.

[16] Y. Saad, J. R. Chelikowsky, and S. M. Shontz, "Numerical methods for electronic structure calculations of materials," *SIAM Review*, vol. 52, no. 1, pp. 3-54, 2010.

[17] M. E. El-Khouly, A. M. Kobaisy, H. Ahmed, M. M. El-Hendawy, M. Ghali, W. A. El-Said, and T. Mohamed, "Femtosecond nonlinear optical properties of push–pull chromophores using Z-scan technique: experimental and computational studies," *Optical and Quantum Electronics*, vol. 55, no. 11, p. 941, 2023.

[18] K. Priyadharsini, A. B. Dileepan, R. Ramasamy, R. V. Solomon, N. Arumugam, A. I. Almansour, and S. Jeyaram, "Observation of Fascinating Nonlinear Optical Features of Fluorescent Dye in Selected Polar Solvents by Z-Scan and DFT Method," *Journal of Fluorescence*, pp. 1-12, 2025.

[19] J. R. Reimers, *Computational methods for large systems: electronic structure approaches for biotechnology and nanotechnology*. John Wiley & Sons, 2011.

[20] X. Wu, S. N. Steinmann, and C. Michel, "Gaussian attractive potential for carboxylate/cobalt surface interactions," *The Journal of Chemical Physics*, vol. 159, no. 16, 2023.

[21] S. Kilina, D. Kilin, and S. Tretiak, "Light-driven and phonon-assisted dynamics in organic and semiconductor nanostructures," *Chemical Reviews*, vol. 115, no. 12, pp. 5929-5978, 2015.

[22] P. Sharma, "Temperature-dependent probing of transport and nonlinear optical properties of topological materials," Doctoral dissertation, RMIT University, 2024.

[23] A. Kanaani, D. Ajloo, H. Kiyani, H. Ghasemian, M. Vakili, and M. Feizabadi, "Molecular structure, spectroscopic investigations and computational study on the potential molecular switch of (E)-1-(4-(2-hydroxybenzylideneamino) phenyl) ethanone," *Molecular Physics*, vol. 114, no. 13, pp. 2081-2097, 2016.